Surface Radiative Transfer in Gas-to-Gas Cocurrent Microheat Exchanger

Shripad P. Mahulikar
Dept. of Aerospace Engineering, Indian Institute of Technology Bombay, IIT Powai, Mumbai 400076, India

Heinz Herwig
Instituts für Thermofluiddynamik, Technische Universität Hamburg-Harburg, Denickestr. 17, D-21073 Hamburg, Germany

Jing-Wei Zhou
College of Metrology and Measurement Engineering, China Jiliang University, Hangzhou 310018, P.R. China

Yash M. Sodhani
Dept. of Aerospace Engineering, Indian Institute of Technology Bombay, IIT Powai, Mumbai 400076, India

DOI 10.1002/aic.12250
Published online April 22, 2010 in Wiley Online Library (wileyonlinelibrary.com).

The influence of surface radiative transfer in parallel flow microheat exchanger is numerically studied for its importance at high temperatures and for small flow dimensions. For these heat exchangers, the role of radiation is beneficial when the convective heat transfer to the annulus flow exceeds the convective heat transfer from the core flow. For this case, radiation improves the heat exchanger performance by decreasing the logarithmic mean temperature difference and by increasing the capacity, effectiveness, and volumetric heat transfer coefficient. Additional surface area is made available for convection to the annulus flow, thereby increasing the specific heat transfer surface for fixed geometry. Therefore, a high emissivity layer over the surfaces of microheat exchanger can improve the heat exchange performance. The active heat transfer area weighted by the convective heat flow rates is introduced as the true measure of heat exchanger compactness. © 2010 American Institute of Chemical Engineers *AIChE J,* 57: 40–50, 2011

Keywords: microheat exchanger, radiative transfer, volumetric heat transfer coefficient

Introduction

Microheat exchangers have at least one fluid flow passage with typical dimension between 1 μm and 1 mm and have great potential in process intensification of various industrial areas.[1] For constant Nu and k, the convection coefficient, $h_c \propto D_h^{-1}$; and the ratio, (wetted area/volume) $\propto D_h^{-1}$, where, the wetted area includes the heat transfer area of heat exchanger. Hence, the volumetric heat transfer coefficient improves toward the microscale[2]; implying efficient use of material, volume, and energy in microheat exchangers.[3] Microheat exchangers find applications in several important fields, e.g., aerospace, bioengineering, cooling of gas turbine blades/infrared detectors/powerful laser mirrors/superconductors, microelectronics, and thermal control of film deposition. High-temperature and compact microheat exchangers can be manufactured using the ceramic tape technology[4] that uses fused ceramic layers, which can create channels with dimensions below 1 mm.[5] Metal-based microchannel heat exchangers are also of contemporary interest because of the combination of high heat transfer performance and improved mechanical integrity.[6]

Correspondence concerning this article should be addressed to S. P. Mahulikar at spm@aero.iitb.ac.in.

Performance of heat exchanger

The price for increasing thermal efficiency of heat exchangers is more complex channel geometry and increase in pressure drop, which can be acceptable if within design limits.[5] Jiang et al.[7] experimentally investigated the fluid flow and forced convection performance of microheat exchangers with microchannels and porous media. They reported that considering heat transfer and pressure drop performance, the microchannel design offers a better overall performance than the porous media. Kang and Tseng[8] developed a theoretical model for predicting the thermal and fluidic performance of a crossflow microheat exchanger. Their analytical results showed that the average temperature of the hot and cold side flow significantly affect the heat transfer rate for the same effectiveness (η). The numerical simulation by Hasan et al.[9] revealed that the size and shape of channels of microheat exchanger can have considerable effect on their performance for the same volume. They found that increasing the number of channels increases the thermal performance, and channels with circular cross-section give the best overall performance (thermal and hydraulic).

Heat exchanger performance is degraded by nonuniformities in inlet fluid flow and temperature on both hot and cold fluid sides.[10] These nonuniformities are generally associated with: (*i*) improper entrance configuration due to poor header design; and (*ii*) imperfect passage-to-passage flow distribution in a highly compact heat exchanger, caused by manufacturing tolerances. Low thermal conductivity (k) Fouling layers are also associated with degradation of thermal performance. Therefore, numerical estimation of 3D Fouling layer profiles for the optimization of cleaning schedules has been investigated,[11] as an alternative to ultrasonic waves fouling detection techniques.

The experimental results of Alm et al.[12] showed the limits of liquid-phase applications in the low-temperature range at high mass flow rate, $\dot{m}$. They suggested that further research should focus on performance prediction in high temperature applications with gaseous media. Kwon et al.[13] experimentally investigated the Internal Heat Exchanger (IHX) for CO_2 pump system. They reported that for the same $\dot{m}$, the capacity and effectiveness (η) increase with IHX length and hot-side inlet temperature. Miwa et al.[14] numerically studied the performance of gas-to-gas microheat exchangers without considering surface radiative transfer, in plane channels with heights in the range 10–100 μm. They reported that for the case of parallel-flow, η can exceed unity under certain conditions, determined by the exit Mach numbers of hot and cold flows.

The performance of heat exchanger is also sensitive to the effects of fluid property variations[15] and parasitic heat losses to the environment (e.g., radiation). Peterson and Vanderhoff[16] modeled the losses in bayonet-type counter-flow heat exchanger because of nonunity effectiveness, axial conduction, and radiation to the surroundings. Axial conduction and radiation losses were found to be significant in small-scale and high-temperature heat exchangers. Nellis[17] reported that radiation is a significant loss mechanism for heat exchangers with high effectiveness and spanning a small temperature range. It was found that the performance of the heat exchanger is degraded by imposing the radiation on the hot rather than the cold fluid side. Offset plates are used as interrupted fin surfaces in compact heat exchangers in many industrial applications for promoting h_c by hindering flow development.[18] Ali et al.[19] numerically investigated laminar-forced convective heat transfer of air flow in a two parallel plate channel with offset plates heated by radiation heat flux. They used the ray tracing technique followed by a series analysis to obtain the net absorbed radiation fractions in the boundary elements. The view factors between surfaces were estimated using the general relation for two infinitely long and directly opposed parallel plates of the same finite width.

High axial conduction is undesirable; hence, very high conducting materials are not the prime choice for microheat exchangers; instead, optimal conductivity is provided by ceramics (e.g., SiC). The experimental results of Bier et al.[20] showed that stainless steel ($k_w \sim 15$ W/m K) yields much higher performance than copper ($k_w \sim 401$ W/m K), when fluids with low heat capacities are used. For low flow rates, they measured, greatly reduced overall heat transfer coefficients compared with the values expected for laminar flow. Stief et al.[21] numerically found that reduction of thermal conductivity of the wall material (k_w) up to an optimum can improve the heat exchanger performance, for given wall thickness. Maranzana et al.[22] proposed a dimensionless axial conduction number for quantifying axial conduction in the walls. They analytically found that wall axial conduction lowers the effectiveness and turns the counter-flow heat exchanger into a mixer, i.e., tendency toward equalization of outlet fluid temperatures. Meschke et al.[23] experimentally and numerically studied the heat transfer performance of a first-hour cross-flow micro-SiC heat exchanger with a diameter of 68 mm, using N_2-gas flows. They reported that the high k of sintered SiC ($\sim$125 W/m K, close to the optimum) results in a superior gas-to-gas heat transfer and a reasonable efficiency at high loads.

Motivation

There are no investigations that examine the role of surface radiation exchange in gas-to-gas microheat exchangers, used e.g., for heat recovery of hot exhaust air and in microreactors.[14] The role of radiation in heat exchangers becomes important because of fouling, which increases the surface emissivity. A growing fouling layer influences surface radiation much earlier than the effect in increasing the thermal resistance. High-performance microheat exchangers have dimensions that approach the microscale and the difference between hot and cold fluid temperatures is typically large. Therefore, the axial fluid and wall temperature gradients are large (e.g., Mahulikar and Herwig[24] for variations of axial relative to radial fluid temperature gradients, from macro-to-microscale). Therefore, for radiation modeling, the wall surfaces cannot be approximated as infinitely long coaxial cylinders; instead they must be axially discretized for capturing the variations.

Objectives and scope

The link from microscales to macroscales through several intermediate scales is resolved using fractal and constructal approaches.[25] It is also important to identify nonrarefaction effects that increasingly surface from the macroscale to the

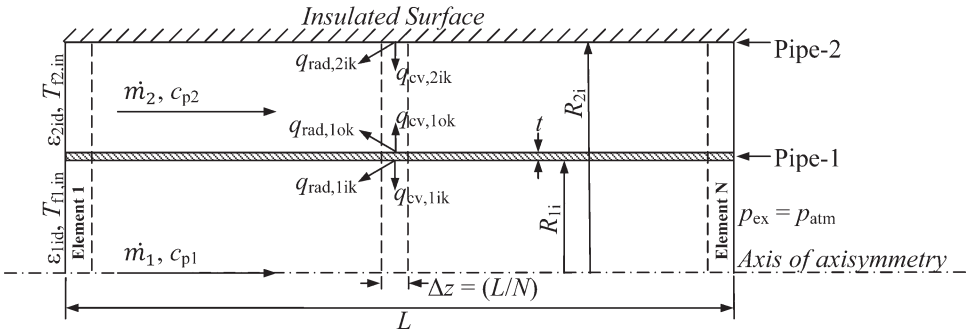

Figure 1. Schematic of discretized tubular co-current heat exchanger.

microscale,[26] to explore their role in the performance. It is inferred from the study of Rachkovskij et al.[27] that as the heat exchanger size decreases, attention must be focussed on the resulting change in the character of heat exchange. In this investigation, surface radiative transfer is studied as a nonrarefaction effect for its significance in gas-to-gas parallel-flow microheat exchangers. As heat exchangers with dimensions approaching the microscale are studied, the effect of gas radiation is unimportant due to the small optical path-lengths.

Modeling of combined convective and surface radiative heat transfer

A parallel flow heat exchanger composed of an inner pipe embedded in a larger diameter coaxial pipe is studied (Figure 1). The outer pipe wall (2) is assumed to be perfectly insulated, because ideally heat exchange is to be achieved with minimal heat loss to the surroundings; i.e., $q_{cv,2ok} = q_{rad,2ok} = 0$. Because of direct radiant heat exchange between the outer surface of pipe 1 and inner surface of pipe 2, $T_{w,2k} \neq T_{f,2k}$; hence, $q_{cv,2ik} \neq 0$ and $q_{rad,2ik} \neq 0$. In the classical heat exchanger problem with only convective mode of heat transfer, $T_{w,2k} = T_{f,2k}$, i.e., $q_{cv,2ik} = 0$. The inner pipe wall (1) of the heat exchanger is thin ($t_1 = 50$ μm) and of high enough thermal conductivity so that, $Bi \ll 1$. Therefore, its inner and outer surface temperatures are identical, because of the desired high radial heat conduction. But because of the small thickness, heat conduction resistance in the radial direction is much smaller than in the axial direction; hence, axial conduction is considered insignificant. These assumptions preclude heat conduction modeling for the inner wall, thereby enabling the study of characteristics of surface radiative transfer.

The parallel flow heat exchanger is axially discretized into N number of elements of equal width, $\Delta z = (L/N)$, as shown in Figure 1. Each element, k $\{\forall\ k \in [1,N]\}$, is assigned with unknown convective and radiative heat flow rates at, $z_k = (k-{}^1/_2)\cdot\Delta z$, which are expressed in terms of fluid and wall temperatures. Using energy conservation principle for steady state and definitions of heat flow rate terms in the conservation equations, a system of nonlinear algebraic equations are obtained.

Equations for an element of discretized heat exchanger

By energy conservation for steady state, the algebraic sum of heat flow rates because of convection and radiation from the inner pipe (1) wall leads to no accumulation of internal energy of the wall. Therefore,

$$q_{cv,1ik} + q_{cv,1ok} + q_{rad,1ik} + q_{rad,1ok} = 0; \tag{1}$$

where, the heat flow rates leaving the wall surface, as indicated in Figure 1, are considered positive. By definition,

$$q_{cv,1ik} = h_{1ik} \cdot A_{1ik} \cdot (T_{w,1k} - T_{fm,1k}), \tag{1.1}$$

$$q_{cv,1ok} = h_{1ok} \cdot A_{1ok} \cdot (T_{w,1k} - T_{fm,2k}), \tag{1.2}$$

and

$$q_{rad,1ik} = A_{1ik} \cdot (B_{1ik} - H_{1ik}). \tag{1.3}$$

The radiance and irradiance are, respectively, given as,

$$B_{1ik} = \varepsilon_{1ik} \cdot \sigma \cdot T_{w,1k}^4 + (1 - \varepsilon_{1ik}) \cdot H_{1ik}, \tag{1.3.1}$$

and

$$H_{1ik} = F_{1ik-1id} \cdot B_{1id} + \sum_{j=1}^{N} (F_{1ik-1ij} \cdot B_{1ij}) + F_{1ik-1ed} \cdot \sigma \cdot T_{\infty}^4. \tag{1.3.2}$$

By definition,

$$q_{rad,1ok} = A_{1ok} \cdot (B_{1ok} - H_{1ok}), \tag{1.4}$$

where,

$$B_{1ok} = \varepsilon_{1ok} \cdot \sigma \cdot T_{w,1k}^4 + (1 - \varepsilon_{1ok}) \cdot H_{1ok}, \tag{1.4.1}$$

and

$$H_{1ok} = F_{1ok-2id} \cdot B_{2id} + \sum_{j=1}^{N} (F_{1ok-2ij} \cdot B_{2ij}) + F_{1ok-2ed} \cdot \sigma \cdot T_{\infty}^4. \tag{1.4.2}$$

Similarly by using energy conservation for steady state for the outer pipe (2) wall,

$$q_{cv,2ik} + q_{rad,2ik} = 0; \tag{2}$$

where,

$$q_{cv,2ik} = h_{2ik} \cdot A_{2ik} \cdot (T_{w,2k} - T_{fm,2k}), \tag{2.1}$$

$$q_{\mathrm{rad,2ik}} = A_{\mathrm{2ik}} \cdot (B_{\mathrm{2ik}} - H_{\mathrm{2ik}}), \tag{2.2}$$

$$B_{\mathrm{2ik}} = \varepsilon_{\mathrm{2ik}} \cdot \sigma \cdot T_{\mathrm{w,2k}}^4 + (1 - \varepsilon_{\mathrm{2ik}}) \cdot H_{\mathrm{2ik}}, \tag{2.2.1}$$

and

$$H_{\mathrm{2ik}} = F_{\mathrm{2ik-2id}} \cdot B_{\mathrm{2id}} + \sum_{\mathrm{j=1}}^{\mathrm{N}} (F_{\mathrm{2ik-1oj}} \cdot B_{\mathrm{1oj}} + F_{\mathrm{2ik-2ij}} \cdot B_{\mathrm{2ij}}) + F_{\mathrm{2ik-2ed}} \cdot \sigma \cdot T_{\infty}^4. \tag{2.2.2}$$

The enthalpy change of air flowing in the inner pipe is due to heat received by convection, i.e.,

$$\dot{m}_1 \cdot [c_{\mathrm{p1}}(T_{\mathrm{fm,1k}}) \cdot T_{\mathrm{0fm,1k}} - c_{\mathrm{p1}}(T_{\mathrm{fm,1(k-1)}}) \cdot T_{\mathrm{0fm,1(k-1)}}] = q_{\mathrm{cv,1ik}}, \tag{3}$$

where,

$$T_{\mathrm{0fm,1k}} = [c_{\mathrm{p1}}(T_{\mathrm{fm,1k}}) \cdot T_{\mathrm{fm,1k}} + u_{\mathrm{m,1k}}^2/2]/c_{\mathrm{p1}}(T_{\mathrm{0fm,1k}}), \tag{3.1}$$

$$u_{\mathrm{m,1k}} = u_{\mathrm{m,1(k-1)}} \cdot (\rho_{\mathrm{1(k-1)}}/\rho_{\mathrm{1k}}), \tag{3.1.1}$$

$$\rho_{\mathrm{1k}} = p_{\mathrm{1k}}/(R_{\mathrm{g1}} \cdot T_{\mathrm{fm,1k}}), \tag{3.1.2}$$

and

$$p_{\mathrm{1k}} = p_{\mathrm{1(k+1)}} + [(8\mu_{\mathrm{1k}} \cdot u_{\mathrm{m1,k}} \cdot \Delta z)/R_1^2] + \rho_{\mathrm{m1}} \cdot u_{\mathrm{m1}} \cdot (u_{\mathrm{m1,k+1}} - u_{\mathrm{m1,k}}). \tag{3.1.3}$$

Similarly,

$$\dot{m}_2 \cdot [c_{\mathrm{p2}}(T_{\mathrm{fm,2k}}) \cdot T_{\mathrm{0fm,2k}} - c_{\mathrm{p2}}(T_{\mathrm{fm,2(k-1)}}) \cdot T_{\mathrm{0fm,2(k-1)}}] = q_{\mathrm{cv,1ok}} + q_{\mathrm{cv,2ik}}, \tag{4}$$

$$T_{\mathrm{0fm,2k}} = [c_{\mathrm{p2}}(T_{\mathrm{fm,2k}}) \cdot T_{\mathrm{fm,2k}} + u_{\mathrm{m,2k}}^2/2]/c_{\mathrm{p2}}(T_{\mathrm{0fm,2k}}), \tag{4.1}$$

$$u_{\mathrm{m,2k}} = u_{\mathrm{m,2(k-1)}} \cdot (\rho_{\mathrm{2(k-1)}}/\rho_{\mathrm{2k}}), \tag{4.1.1}$$

$$\rho_{\mathrm{2k}} = p_{\mathrm{2k}}/(R_{\mathrm{g2}} \cdot T_{\mathrm{fm,2k}}), \tag{4.1.2}$$

and

$$p_{\mathrm{2k}} = p_{\mathrm{2(k+1)}} + \frac{8\mu_{\mathrm{2k}} \cdot u_{\mathrm{m2,k}} \cdot \Delta z}{R_2^2 \cdot \left(1 + \kappa^2 + \frac{1-\kappa^2}{\ln(\kappa)}\right)} + \rho_{\mathrm{m2}} \cdot u_{\mathrm{m2}} \cdot (u_{\mathrm{m2,k+1}} - u_{\mathrm{m2,k}}). \tag{4.1.3}$$

Equations 3.1 and 4.1 are based on thermally perfect model for obtaining T_{0fm} from the static temperature T_{fm}. The temperatures in the brackets after c_{p} in Eqs. 3, 3.1, 4, and 4.1, denote the mathematical function. The expressions for pressure drop due to fluid friction in Eq. 3.1.3 and 4.1.3 are based on laminar fully developed velocity profiles, which are more justified toward the microscale.[27] In circular tube flow, the velocity profile is the classical parabolic, and its expression for annulus flow is given by Kadaner et al.[28] For the temperature range, 273–550 K, average value of $c_{\mathrm{p}} = 1018.2$ J/kg K is used, because the variation is less than 3%. For the range, 550–2100 K, $c_{\mathrm{p}}(T)$-variation for air is obtained by least-square error 4th order polynomial fit to the data[29] as, $c_{\mathrm{p}}[T(\mathrm{K})] = a_{\mathrm{o}} + a_1 T + a_2 T^2 + a_3 T^3 + a_4 T^4$ J/kg K. The coefficients are as follows: $a_{\mathrm{o}} = 874.687$, $a_1 = 0.325431$, $a_2 = -2.07132 \times 10^{-5}$, $a_3 = -6.63386 \times 10^{-8}$, $a_4 = 2.66353 \times 10^{-11}$.

Equations for inlet disks

In Eq. 1.3.2, 1.4.2, and 2.2.2, additional unknowns for the radiances from the two inlet disks, 1id and 2id, are introduced. The radiance from the circular disk at the inlet of the inner cylinder (1) of radius R_{i} is given as,

$$B_{\mathrm{1id}} = \varepsilon_{\mathrm{1id}} \cdot \sigma \cdot T_{\mathrm{1id}}^4 + (1 - \varepsilon_{\mathrm{1id}}) \cdot H_{\mathrm{1id}}, \tag{5}$$

where,

$$H_{\mathrm{1id}} = \sum_{k=1}^{\mathrm{N}} (F_{\mathrm{1id-1ik}} \cdot B_{\mathrm{1ij}}) + F_{\mathrm{1id-1ed}} \cdot \sigma \cdot T_{\infty}^4. \tag{5.1}$$

Similarly,

$$B_{\mathrm{2id}} = \varepsilon_{\mathrm{2id}} \cdot \sigma \cdot T_{\mathrm{2id}}^4 + (1 - \varepsilon_{\mathrm{2id}}) \cdot H_{\mathrm{2id}}, \tag{6}$$

and

$$H_{\mathrm{2id}} = \sum_{k=1}^{\mathrm{N}} (F_{\mathrm{2id-1ok}} \cdot B_{\mathrm{1ok}} + F_{\mathrm{2id-2ik}} \cdot B_{\mathrm{2ik}}) + F_{\mathrm{2id-2ed}} \cdot \sigma \cdot T_{\infty}^4. \tag{6.1}$$

Boundary conditions and inputs

(i) At the inlet, the flow velocities and temperatures are specified as, $u_{\mathrm{m1}}(z = 0) = u_{\mathrm{m1,in}}$, $u_{\mathrm{m2}}(z = 0) = u_{\mathrm{m2,in}}$, $T_{\mathrm{fm1}}(z = 0) = T_{\mathrm{fm1,in}}$, and $T_{\mathrm{fm2}}(z = 0) = T_{\mathrm{fm2,in}}$. The temperatures of the inlet disks, which are required for radiation interchange calculations, are considered the same as the inlet air temperatures; i.e. $T_{\mathrm{1id}} = T_{\mathrm{fm1,in}}$ and $T_{\mathrm{2id}} = T_{\mathrm{fm2,in}}$.

(ii) At the exit, the static pressures are specified as, $p_{\mathrm{1,ex}}(z = L) = p_{\mathrm{atm}}$, and $p_{\mathrm{2,ex}}(z = L) = p_{\mathrm{atm}}$. The two exit disks, 1ed and 2ed, are considered to be at ambient temperatures, i.e. $T_{\mathrm{1ed}} = T_{\mathrm{2ed}} = T_{\infty}$.

(iii) The emissivities of all surfaces, $\varepsilon_{\mathrm{1ik}}$, $\varepsilon_{\mathrm{1ok}}$, $\varepsilon_{\mathrm{2ik}}$, $\{\forall\ k \in [1,\mathrm{N}]\}$, $\varepsilon_{\mathrm{1id}}$, and $\varepsilon_{\mathrm{2id}}$, are specified. The exit disks are considered as black surfaces, because the heat exchanger is considered open to the ambient at the exit-plane. The role of radiation can be switched-off by making all these emissivities zero, including those of the exit disks.

(iv) The details of the view factors in irradiance equations are listed in Table 1.[30]

Numerical solution scheme

The system of 24 algebraic Eqs. 1–4.1.3 for the kth element have the following 24 unknowns: $T_{\mathrm{fm,1k}}$, $T_{\mathrm{fm,2k}}$, $T_{\mathrm{w,1k}}$, $T_{\mathrm{w,2k}}$, $q_{\mathrm{cv,1ik}}$, $q_{\mathrm{cv,1ok}}$, $q_{\mathrm{cv,2ik}}$, $q_{\mathrm{rad,1ik}}$, $q_{\mathrm{rad,1ok}}$, $q_{\mathrm{rad,2ik}}$, $T_{\mathrm{0fm,1k}}$, $T_{\mathrm{0fm,2k}}$, $u_{\mathrm{m,1k}}$, $u_{\mathrm{m,2k}}$, ρ_{1k}, ρ_{2k}, p_{1k}, p_{2k}, B_{1ik}, B_{1ok} B_{2ik}, H_{1ik}, H_{1ok}, H_{2ik}. Also, there are 4 unknowns for the two inlet disks, viz. B_{1id}, H_{1id}, B_{2id}, H_{2id}; refer Eqs. 5–6.1. Hence, there are $24N+4$ nonlinear algebraic equations in $24N+4$ unknowns, which are numerically solved by the Newton–Raphson method. In this iterative procedure, all equations are expanded in the form of linear Taylor's series and higher order terms are not considered. The Jacobian matrix of the system of equations is arranged for obtaining its diagonal

Table 1. Radiation View Factors Required in Irradiance Equations

$F_{i\text{-}j}$	*Eq.*	Description
(a) View Factors Without Partially Obstructed Visibility		
$F_{1ik\text{-}1id}$	1.3.2	Inner surface of k^{th} element of Pipe-1 of inner radius R_{1i} and width Δz (surface: 1*ik*) as seen by circular inlet disk surface of Pipe-1 of radius R_{1i} (surface: 1*id*).
$F_{1id\text{-}1ik}$	5.1	Obtained using reciprocal rule from $F_{1ik\text{-}1id}$.
$F_{1ik\text{-}1ed}$	1.3.2	Surface 1*ik* as seen by circular exit disk surface of Pipe-1 (surface: 1*ed*); identical to, $F_{1ik\text{-}1id}$.
$F_{1ik\text{-}1ij}$	1.3.2	Surface 1*ik* as seen by inner surface of *j*th element of Pipe-1 (surface: 1*ij*), both of inner radius R_{1i} and width Δz.
$F_{1id\text{-}1ed}$	5.1	Surface 1*id* as seen by Surface 1*ed*.
$F_{1ok\text{-}2id}$	1.4.2	Outer surface of k^{th} element of Pipe-1 of outer radius R_{1o} and width Δz (surface: 1*ok*) as seen by annular inlet disk surface with inner & outer radii = R_{1o} & R_{2i}, at inlet of annulus (surface: 2*id*).
$F_{1ok\text{-}2ed}$	1.4.2	Surface 1*ok* as seen by annular exit disk surface with inner & outer radii = R_{1o} & R_{2i}, respectively, at exit of annulus (surface: 2*ed*); identical to $F_{1ok\text{-}2id}$.
$F_{2id\text{-}1ok}$	6.1	Obtained using reciprocal rule from $F_{1ok\text{-}2id}$.
$F_{1ok\text{-}2ij}$	1.4.2	Surface 1*ok* as seen by inner surface of j^{th} element of outer pipe of inner radius R_{2i} and width Δz (surface: 2*ij*).
$F_{2ik\text{-}1oj}$	2.2.2	Obtained using reciprocal rule from $F_{1oj\text{-}2ik}$.
(b) View Factors with Partially Obstructed Visibility by Inner Pipe of Outer Radius R_{1o}		
$F_{2ik\text{-}2id}$	2.2.2	Inner surface of k^{th} element of outer pipe of inner radius R_{2i} and width Δz (2*ik*) as seen by the annular inlet disk surface (inner radius = R_{1o} & outer radius = R_{2i}) at inlet of annulus (2*id*).
$F_{2id\text{-}2ik}$	6.1	Obtained using reciprocal rule from $F_{2ik\text{-}2id}$.
$F_{2ik\text{-}2ed}$	2.2.2	Surface 2*ik* as seen by annular exit disk surface (inner radius = R_{1o} & outer radius = R_{2i}) at exit of annulus (2*ed*); identical to $F_{2ik\text{-}2id}$.
$F_{2ik\text{-}2ij}$	2.2.2	Surface 2*ik* as seen by inner surface of j^{th} element of outer pipe (2*ij*), both of inner radius R_{2i} and width Δz.
$F_{2id\text{-}2ed}$	6.1	Surface 2*id* as seen by Surface 2*ed*.

dominance. Therefore, each unknown variable is obtained directly from its previous value, without solving a system of linear algebraic equations in every iteration.

Numerical Simulation and Results

The energy balance error,

$$\delta_E = (|\dot{E}_{in} - \dot{E}_{ex}|/\dot{E}_{in}) \times 100\%, \tag{7}$$

is monitored for all cases presented with $N = 100$, where, $\delta_{E,max} < 5\%$. In this investigation, the maximum error is for the highest value of $T_{fm1,in}$ (=1400°C). In Eq. 7,

$$\dot{E}_{in} = \dot{m}_1 \cdot c_{p1} \cdot T_{0fm1,in} + \dot{m}_2 \cdot c_{p2} \cdot T_{0fm2,in} + A_{1id} \cdot B_{1id} + \cdot A_{2id} \cdot B_{2id}, \tag{7.1}$$

$$\dot{E}_{ex} = \dot{m}_1 \cdot c_{p1} \cdot T_{0fm1,ex} + \dot{m}_2 \cdot c_{p2} \cdot T_{0fm2,ex} + A_{1ed} \cdot H_{1ed} + \cdot A_{2ed} \cdot H_{2ed}, \tag{7.2}$$

where,

$$H_{1ed} = F_{1ed-1id} \cdot B_{1id} + \sum_{j=1}^{N} (F_{1ed-1ij} \cdot B_{1ij}), \tag{7.2.1}$$

and

$$H_{2ed} = F_{2ed-2id} \cdot B_{2id} + \sum_{j=1}^{N} (F_{2ed-1oj} \cdot B_{1oj} + F_{2ed-2ij} \cdot B_{2ij}). \tag{7.2.2}$$

In Eq. 7.2, $T_{0fm1,ex}$ and $T_{0fm2,ex}$ are obtained by linear extrapolation from their known values at $z = (N-{}^1/_2)\cdot\Delta z$ and at $z = (N-{}^3/_2)\cdot\Delta z$.

The summation rule for view factors in an enclosure is checked and the following summations are found to be unity, regardless of the value of N:

$$a)\ F_{1id-1ed} + \sum_{j=1}^{N} F_{1id-1ij} = 1, \quad \text{and}$$

$$b)\ F_{2id-2ed} + \sum_{j=1}^{N} (F_{2id-2ij} + F_{2id-1oj}) = 1; \forall\ k \in [1, N]:$$

$$c)\ F_{1ik-1id} + F_{1ik-1ed} + \sum_{j=1}^{N} F_{1ik-1ij} = 1,$$

$$d)\ F_{1ok-2id} + F_{1ok-2ed} + \sum_{j=1}^{N} F_{1ok-2ij} = 1, \quad \text{and}$$

$$e)\ F_{2ik-2id} + F_{2ik-2ed} + \sum_{j=1}^{N} (F_{2ik-2ij} + F_{2ik-1oj}) = 1.$$

Input data, grid independence study, and results for representative case

Grid independency is studied by increasing N and monitoring the Logarithmic Mean Temperature Difference (LMTD = ΔT_{mean}) for test case with the following input parameters:

$$R_{1i} = 2.5\,\text{mm}, t_1 = 50\,\mu\text{m} (R_{1o} = 2.55\,\text{mm}), R_{2i} = 3.55\,\text{mm} (d_{ann} = 1\,\text{mm}), L = 20\,\text{cm};$$

$T_{fm1,in} = T_{1id} = 1200$°C (hot core-flow), $T_{fm2,in} = T_{2id} = T_\infty = 15$°C (cold annulus-flow);

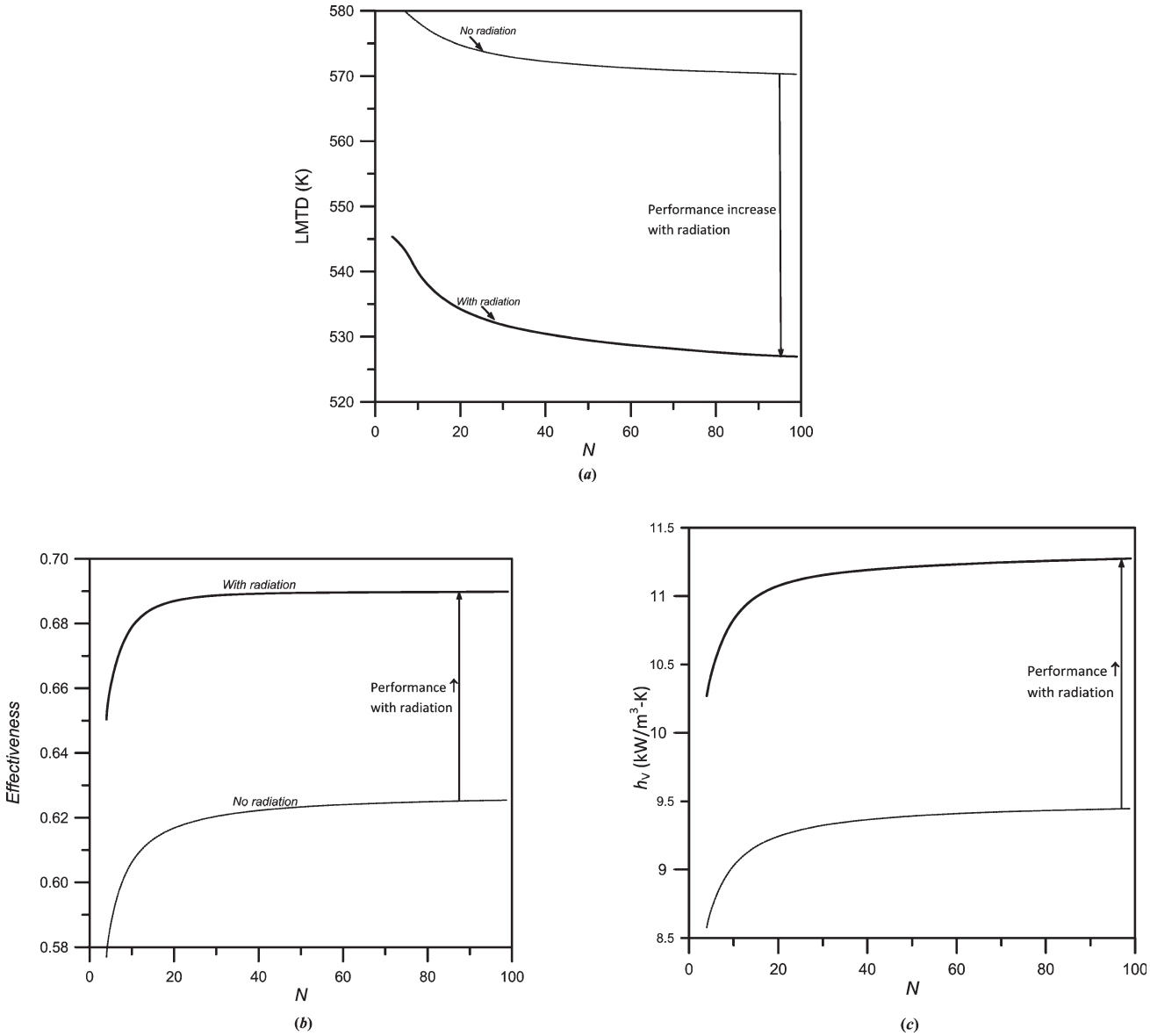

Figure 2. Illustration of grid convergence and benign role of radiation in micro heat exchanger (a) LMTD vs. *N*, (b) η vs. *N*, (c) h_V vs. *N*.

$\varepsilon_{1id} = \varepsilon_{2id} = \{\varepsilon_{1ik} = \varepsilon_{1ok} = \varepsilon_{2ik}(\forall\ k \in [1, \mathrm{N}])\} = 0.9,$
$\varepsilon_{1ed} = \varepsilon_{2ed} = 1;$

$u_{m1,in} = u_{m2,in} = 10\,\mathrm{m/s}; \quad \dot{m}_1 = 47.1\,\mathrm{mg/s},$
$\dot{m}_2 = 235.3\,\mathrm{mg/s}; \quad Re_{D1,in} = 229.9, Re_{D2,in} = 1374.6;$
$p_{1,ex} = p_{2,ex} = p_\infty = 1.01325 \times 10^5\mathrm{Pa}.$

The configuration of hot core-flow and cold annulus-flow is considered as test case, because it is practically easier to provide insulation over the cold annulus-flow than over the hot annulus-flow.

The convection coefficients, $h_{c,1ik}$, $h_{c,1ok}$, and $h_{c,2ik}$ $\{\forall\ k \in [1,N]\}$, are obtained from, $h_c(z) = Nu_T{\cdot}k[T_{fm}(z)]/D_h$; where, for Pipe-1, $D_h = D_{1i}$, and for Pipe-2, $D_h = D_{2i} - D_{1o}$. In parallel flow exchanger, $T_{fm}(z)$-variation is closer to T_w = const. wall boundary condition (exponential variation) than to 'q''_w = const. boundary condition; hence, $Nu_T = 3.66$. For nonreacting air,[29] $k(T) = \frac{1.9942\times10^{-3}T^{1.5}}{T+112}$ W/m K and because $(\partial k/\partial T) > 0$, $h(z)$ increases along the flow for cold flow and decreases along the flow for hot flow. The LMTD is given as,[31]

$$\Delta T_{mean} = (\Delta T_{in} - \Delta T_{ex})/\ln(\Delta T_{in}/\Delta T_{ex}); \tag{8}$$

which, for a given configuration with fixed flow is a measure of the amount of heat exchange. Thus, lower LMTD indicates higher volumetric heat transfer coefficient (h_V) and effectiveness, given as,[31]

$$\eta = q_{actual}/q_{max}. \tag{9}$$

Figure 2(a) gives the variation of ΔT_{mean} with N for cases with and without radiation; where, in Eq. 8, $\Delta T_{in} = T_{fm1,in}(z = 0) - T_{fm2,in}(z = 0)$ and $\Delta T_{ex} = T_{fm1,ex}(z = L) - T_{fm2,ex}(z$

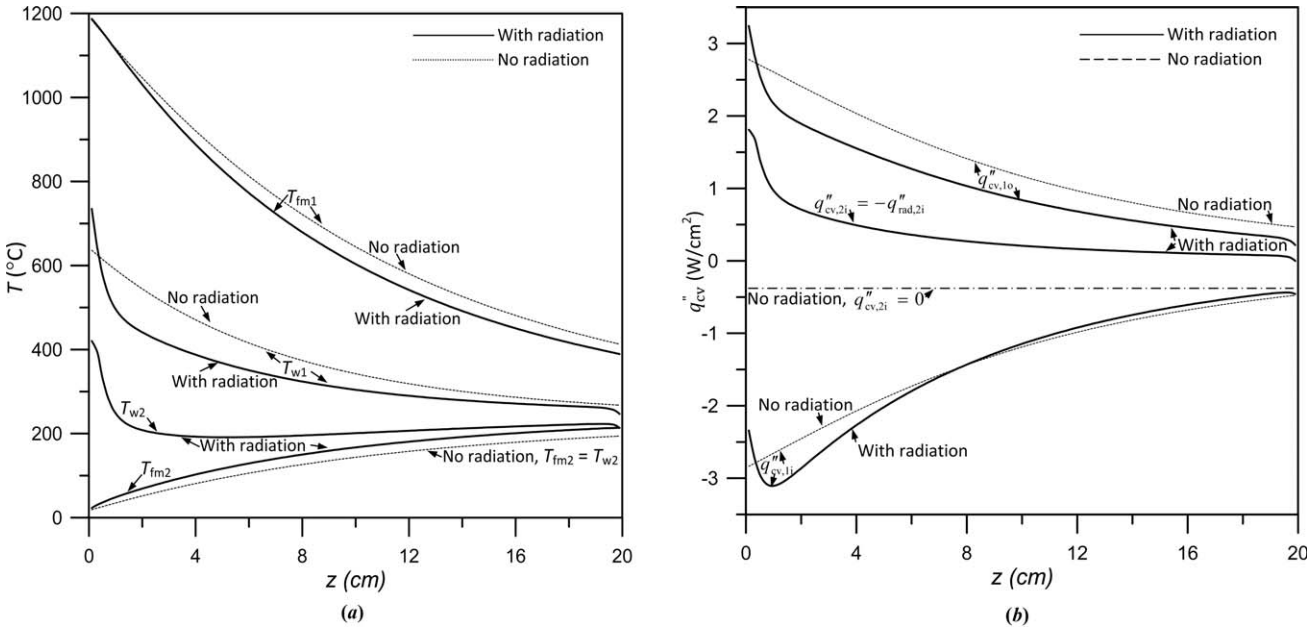

Figure 3. Simulation results for micro heat exchanger with hot core and cold annulus flow (a) *T*(*z*)-variation, with and without radiation (b) q''_{cv} (*z*)-variation, with and without radiation.

$= L$). Radiation lowers LMTD by about 43 K, which for a given heat exchanger configuration is beneficial and not parasitic.[16,17] The variation of η with N for cases with and without radiation is in Figure 2b, where the increased η with radiation confirms the benevolent role of radiation. In Eq. 9, $q_{actual} = q_{cv,1oT} + q_{cv,2iT}$, is the capacity; and $q_{max} = C_{min}\cdot(T_{fm1,in}-T_{fm2,in})$, where, C_{min} is the smaller of $(\dot{m}_1\cdot c_{p1,in})$ and $(\dot{m}_2\cdot c_{p2,in})$. The combined measure of enhanced performance with radiation because of reduced ΔT_{mean} [Eq. (8)] and increased q_{actual} in Eq. 9 is the increased h_V in Figure 2c, given as,[7]

$$h_V = q_{actual}/(V \cdot \Delta T_{mean}). \quad (10)$$

With radiation, and changing N from 80 to 100, ΔT_{mean} changes by less than 0.8 K, η changes by less than 0.02%, and h_V changes by less than 0.17%; therefore, $N = 100$ is fixed for this study.

The temperature variations in Figure 3a explain the decreased LMTD in Figure 2a because of radiation, which lowers $T_{fm,1}(z)$ and increases $T_{fm,2}(z)$, relative to without radiation. The variation of $T_{w1}(z)$ in the vicinity of inlet is significantly affected by the radiant heat exchange with the hot inlet disk, which affects $T_{w2}(z)$-variation close to the inlet. Figure 3b gives the convective heat flux, q''_{cv} (z)-variation, which shows that $q''_{cv,2i} = -q''_{rad,2i} > 0$, and its value is a non-negligible percentage of $q''_{cv,1o}$. The variation in $q''_{cv,1i}$ with and without radiation are identical except in the vicinity of the inlet, where the increase with radiation is due to heat gained by the wall (1i) from the hot inlet disk (1id). Because the area of surface 2i is larger than that of surface 1o by factor, $1+(d_{ann}/R_{1o})$, the effect of radiation on $q_{cv,2iT}$ is even larger.

Analyses of parameters affecting heat exchanger performance due to radiation

Because of direct radiant exchange between the outer surface of inner cylinder and inner surface of outer cylinder, $T_{w,2k} > T_{fm,2k}$; i.e. $q_{cv,2ik} = -q_{rad,2ik} > 0$, $\forall\ k \in [1,N]$. The total convective heat flow from the inner surface of the outer cylinder, $q_{cv,2iT}$, is part of $q_{cv,1iT}$ that is available for heating fluid 2, because of direct radiant exchange between surfaces 1o and 2i. Because additional area of surface *2i* is now available for convective heat transfer to the annulus fluid, radiation makes the heat exchanger effectively more compact

Table 2. Analysis of Surface Radiative Transfer in Performance of Micro Heat Exchanger: Effect of Spacing Reduction

$d_{ann}\downarrow$ (μm)	$u_{m2,in}\uparrow$ (m/s)	$Re_{D2,in}\uparrow$	$\Delta T_{mean}\downarrow$ (K)	$\eta\uparrow$	$h_V\uparrow$ (kW/m^{3}K)	$\lambda_{no\_rad}\uparrow$ (m^{-1})	$\Delta\lambda/\lambda_{no\_rad}\uparrow$
1000*	10.00*	1374.6*	526.9	0.6899	11.275	396.7	7.41%
900	11.29	1397.4	518.7	0.6956	12.227	420.1	7.64%
800	12.91	1421.4	509.7	0.7015	13.308	445.5	7.88%
700	14.99	1445.7	499.7	0.7077	14.547	473.4	8.12%
600	17.77	1471.2	487.9	0.7137	16.005	503.9	8.36%
500	21.63	1497.4	474.6	0.7198	17.693	537.5	8.61%

*Default case [$T_{fm1,in} = 1200$°C, $u_{m1,in} = 10$ m/s: for all cases in Table 2]

Table 3. Analysis of Surface Radiative Transfer in Performance of Micro Heat Exchanger: Effect of Inlet Temperature of Hot Fluid ($T_{fm1,in}$)

$T_{fm1,in}$ ↑	$u_{m1,in}$ ↑	$Re_{D1,in}$ ↓	ΔT_{mean} ↑	η ↑	h_V ↑ (kW/m^3·K)	$\Delta\lambda/\lambda_{no\_rad}$ ↑
1150°C	9.67 m/s	234.7	509.8 K	0.6855	11.019	6.84%
1200°C	10.00 m/s	229.9	526.9 K	0.6899	11.275	7.41%
1250°C	10.34 m/s	225.6	543.4 K	0.6938	11.540	7.99%
1300°C	10.68 m/s	221.5	560.0 K	0.6977	11.808	8.59%
1350°C	11.02 m/s	217.6	576.3 K	0.7014	12.084	9.22%
1400°C	11.36 m/s	214.0	590.1 K	0.7041	12.365	10.4%

for the same geometry. The effective heat transfer area with radiation is,

$$A_{HT} = -A_{1iT} \cdot (q_{cv,1oT} + q_{cv,2iT})/q_{cv,1iT}; \quad (11)$$

where, $A_{1iT} = \pi D_{1i} \cdot L$. The negative sign makes A_{HT} positive, because the signs of $q_{cv,1oT}$ and $q_{cv,2iT}$ are the opposite of $q_{cv,1iT}$. Radiation enhances the compactness if, $q_{cv,1oT} + q_{cv,2iT} > q_{cv,1iT}$ (heat flow rates in this inequality are the magnitudes); in which case, the increase in the effective heat transfer area, $(A_{HT}/A_{1iT})-1$, is a measure of the beneficial role of radiation. The specific heat transfer surface (without radiation) is, $\lambda_{no\_rad} = A_{1iT}/V$, where, the heat exchanger volume, $V = \pi R_2^2 \cdot L$. Hence, the relative increase in the heat transfer area per unit volume is, $(\Delta\lambda/\lambda_{no\_rad}) = (A_{HT}/A_{1iT})-1$; where, the specific heat transfer surface, $\lambda_{HT} = \Delta\lambda + \lambda_{no\_rad}$.

Table 2 shows the effect of reducing d_{ann} from 1.0 to 0.5 mm on ΔT_{mean}, η, h_V, λ_{no_rad}, and λ; i.e., on improving the performance towards the microscale. To maintain the heat capacity of the annulus flow (C_2), i.e., $\dot{m}_2$ same for all these cases, $u_{m2,in}$ is increased from 10.00 to 21.64 m/s, which increases $Re_{D2,in}$ from 1374.6 to 1497.4. Toward microscale annular spacings, λ_{no_rad} increases because V decreases, but $(\Delta\lambda/\lambda_{no\_rad})$ also increases. Therefore, the role of radiation in enhancing the performance increases in conjunction with convection, toward the microscale. The increase in performance of heat exchanger with increasing $T_{fm1,in}$ from 1150 to 1400°C in steps of 50°C, is shown in Table 3. Because the gas density reduces with increasing temperature, $u_{m1,in}$ is increased from 9.67 to 11.36 m/s, to maintain the heat capacity rate (C_1) and $\dot{m}_1$ of the core flow same for all these cases. The increasing ΔT_{mean} from 509.8 to 590.1 K is attributed to the increasing temperature difference between the hot and cold flows. The increase in η from 0.6855 to 0.7041 and increase in h_V from 11.019 to 12.365 indicate that the performance of heat exchanger increases with $T_{fm1,in}$. For $T_{fm1,in} = 1400$°C, the Knudsen number,[32]

$$Kn_{in} = \sqrt{\frac{\pi\gamma}{2}} \cdot \frac{M_{m,in}}{Re_{D,in}}, \quad (12)$$

is the highest ($Kn_{max} = 9.6 \times 10^{-5}$). The Kn for all other cases reported in this investigation is lower than Kn_{max}, thereby justifying the continuum-based approach.

The effect of change in length (L) on performance is in Table 4 in which L is increased from 5 to 35 cm in steps of 5 cm. For all these case, $\lambda_{no\_rad} = 396.7$ m^{-1} = const. but λ_{HT} is higher for shorter heat exchangers. With increasing L, LMTD decreases, because the capacity and η increase, which indicate that the heat exchanger performance increases[13]; but h_V decreases as V increases. Table 5 illustrates the effect of interchanging parameters of hot and cold flows for 4 pairs of cases, (*i*)–(*iv*), for fixed $T_{hot} = 600$°C and $T_{cold} = 15$°C. From cases (*i*)–(*iv*), $\dot{m}_1$ is increased from 47.1 to 235.3 mg/s and $\dot{m}_2$ is decreased from 235.3 to 47.1 mg/s. In cases (*i*) and (*ii*), $\dot{m}_1 < \dot{m}_2$, and in cases (*iii*) and (*iv*), $\dot{m}_1 > \dot{m}_2$; but for all cases, $\dot{m}_1 + \dot{m}_2 = 282.4$ mg/s. In each case, hot fluid flows through the annulus in the first subcase, which has higher η, capacity, and $(\Delta\lambda/\lambda_{no\_rad})$ in cases (*i*) and (*ii*). In cases (*iii*) and (*iv*), the first subcase has lower η and capacity, but higher $(\Delta\lambda/\lambda_{no\_rad})$; thus, η and capacity are superior when larger $\dot{m}$ is hot, i.e., higher role of radiation. Based on η and $(\Delta\lambda/\lambda_{no\_rad})$, the performance is superior for the configuration in which, higher $\dot{m}$ flows through the annulus, which has larger wetted area than the core. For case (*i*), h_v is also higher for the first subcase; therefore, performance is the best when high $\dot{m}_{hot}$ flows through the annulus. The negative sign of $(\Delta\lambda/\lambda_{no\_rad})$ in the 2nd subcase of case (*iv*) indicates that the role of radiation is parasitic.

Figure 4 gives the variations of temperatures and heat fluxes for the 1st subcase of case (*i*) in Table 5, which is the best performance configuration. In Figure 4a, $T_{w1}(z)$ reduces sharply in the vicinity of the exit, because of significant heat loss to the cold exit disks, 1ed and 2ed. Figure 4b gives the convective heat flux, q''_{cv} (z)-variation, which shows that $q''_{cv,2i} = -q''_{rad,2i} < 0$, is a non-negligible percentage of $q''_{cv,1o}$, as in Figure 3b. But the significance of $q''_{cv,2i}$ now is in spite of lower temperature of the hot fluid, relative to Figure 3b. This result is due to the dominant role of surface radiative transfer for the configuration of high hot mass flow through the annulus.

Table 4. Analysis of Surface Radiative Transfer in Performance of Micro Heat Exchanger: Effect of Heat Exchanger Length (L)

L ↑ (cm)	5	10	15	20	25	30	35
ΔT_{mean} ↓ (K)	928.2	748.5	620.8	526.9	455.3	399.4	354.7
η ↑	0.3497	0.5273	0.6290	0.6899	0.7273	0.7510	0.7665
h_V ↓ (kW/m^3·K)	12.975	12.130	11.634	11.275	11.003	10.793	10.626
$(\Delta\lambda/\lambda_{no\_rad})$ ↓	14.80%	9.67%	8.09%	7.41%	7.07%	6.90%	6.83%

Table 5. Analysis of Surface Radiative Transfer in Performance of Micro Heat Exchanger: Effect of Interchanging Parameters of Hot and Cold Flows

Case	$\dot{m}_1$ (mg/s)	$\dot{m}_2$ (mg/s)	$T_{fm1,in}$	$T_{fm2,in}$	η	h_V (kW/m^3·K)	$\Delta\lambda/\lambda_{no\_rad}$
			$\dot{m}_1 < \dot{m}_2$				
i)	47.1	235.3	15°C	600°C	0.7319	9.513	4.69%
			600°C	15°C	0.6361	8.351	2.10%
ii)	94.2	188.2	15°C	600°C	0.4342	8.303	3.24%
			600°C	15°C	0.4195	9.065	1.39%
			$\dot{m}_1 > \dot{m}_2$				
iii)	188.2	94.2	15°C	600°C	0.3677	7.287	2.41%
			600°C	15°C	0.4766	9.918	0.73%
iv)	235.3	47.1	15°C	600°C	0.5775	6.861	1.97%
			600°C	15°C	0.7308	10.039	−0.34%

$\dot{m}_1 + \dot{m}_2 = 282.4$ mg/s.

Conclusions

(i) The performance of parallel flow microheat exchanger with high temperature difference air flows is re-visited, for studying the role of surface radiative transfer. The role of surface radiation interchange in these heat exchangers is found to be beneficial (not parasitic as popularly believed).

(ii) For a given configuration, radiation lowers LMTD, increases both effectiveness and volumetric heat transfer coefficient, all three of which indicate improved performance. Hence, for heat exchangers with dominant role of radiation, it is beneficial to have radiant heat exchange surfaces with higher emissivities. Therefore, the role of thin film of Fouling and high emissivity layer over metallic surfaces of microheat exchanger is to increase the performance.

(iii) The effective heat transfer surface area, which is weighted by the heat flow rates, is introduced as the true measure of compactness of microheat exchanger.

(iv) For a given microheat exchanger geometry, radiation effectively increases the compactness, as additional surface area is available for convective heat transfer to the annulus flow.

(v) The performance of microtubular heat exchanger is best for the configuration in which higher mass flow of hot fluid flows through the annulus. In practice, this configuration would demand more stringent insulation design to reduce the heat loss from the hot annulus flow to the surroundings.

Acknowledgments

The authors thank the A. von Humboldt Foundation, Germany (grant no. 1104249/INI), for the support. The authors also thank the Foreign Experts' Program for Scientific Research, Zhejiang Province, P.R. China (grant no. 2008-607) for the partial support. The authors are grateful to project no. 07IS012 of Department of Aerospace Engg. IIT Bombay, India, for the generous logistic support.

Notation

A = surface area [m^2]
B = radiance from surface [W/m^2]
C = heat capacity rate [W/K]

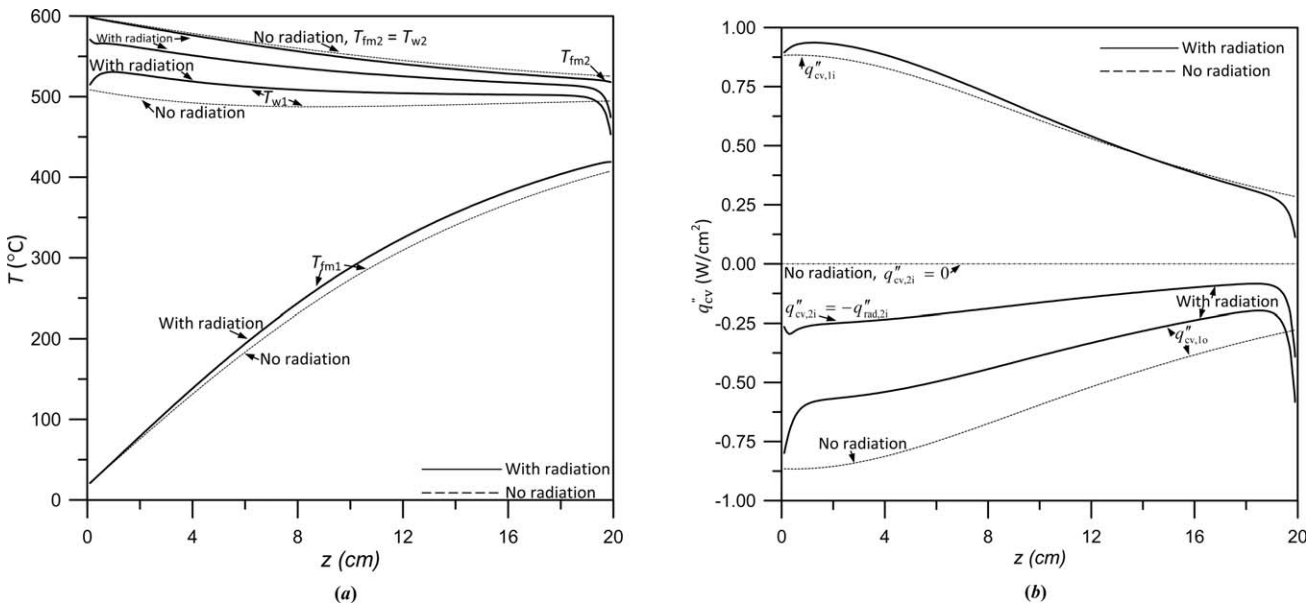

Figure 4. Simulation results for micro heat exchanger with cold core and hot annulus flow (a) $T(z)$-variation, with and without radiation (b) q''_{cv} (z)-variation, with and without radiation.

c_p = specific heat at constant pressure [J/kg K]
D = diameter [m]
d_{ann} = annular spacing between two coaxial cylinders in heat exchanger [m]
$\dot{E}$ = energy flow rate [W]
F_{i-j} = view factor of surface i as seen by surface j
H = irradiance incident on surface [W/m^2]
h_c = convective heat transfer coefficient [W/m^2-K]
h_V = volumetric heat transfer coefficient [W/m^3-K]
k = thermal conductivity [W/m K]
Kn = Knudsen number
L = length of heat exchanger [m]
M = Mach number
$\dot{m}$ = mass flow rate [kg/s]
N = number of axial elements in which heat exchanger is discretized
Nu = Nusselt number
q = heat flow rate [W]
q'' = heat flux [W/m^2]
R = radius of pipe in heat exchanger [m]
Re_D = Reynolds number based on diameter
R_g = specific gas constant [=287.05 J/kg K, for dry air]
t = thickness of inner pipe[1] [m]
T_{fm} = bulk mean fluid temperature [°C, K]
T_w = wall temperature [°C, K]
u = axial flow velocity [m/s]
V = volume of heat exchanger [m^3]
z = flow direction [m]

Greek letters

δ_E = dimensionless energy balance error, see Eq. 7
ΔT_{mean} = Logarithmic Mean Temperature Difference (LMTD) [°C, K]
Δz = width of discretised element [m]
$\Delta\lambda$ = increase in λ due to radiation [m^{-1}]
ε = surface emissivity
γ = ratio of specific heats [=1.4, for dry air]
λ = heat transfer area per unit volume of heat exchanger [m^{-1}]
μ = dynamic viscosity [Pa-s]
ρ = air density [kg/m^3]
σ = Stefan-Boltzmann constant [=5.6704$\times$10^{-8} W/m^2 K^4]

Indexes

cv = convective
ed = exit disk
ex = exit
h = hydraulic
HT = available for heat transfer
i = inner surface
id = inlet disk
in = inlet
k = k^{th} element of discretized heat exchanger layout
m = mean value over cross-section
max = maximum value
no_rad = value of parameter without radiation
o = outer surface
rad = radiative
T = net value for inner / outer surface of cylinder
w = wall
0 = stagnation value
1 = inner pipe / air flow through inner pipe
2 = outer pipe / air flow through annulus
∞ = ambient value

Literature Cited

1. Fan YL, Luo LG. Recent applications of advances in microchannel heat exchangers and multi-scale design optimization. *Heat Transf Eng*. 2008;29:461–474.
2. Schubert K, Brandner J, Fichtner M, Linder G, Schygulla U, Wenka A. Microstructure devices for applications in thermal and chemical process engineering. *Microscale Thermophysical Eng*. 2001;5:17–39.
3. Mehendale SS, Jacobi AM, Shah RK. Fluid flow and heat transfer at micro- and meso-scales with application to heat exchanger design. *Appl Mech Rev*. 2000;53:175–193.
4. Schmitt C, Agar DW, Platte F, Buijssen S, Pawlowski B, Duisberg M. Ceramic plate heat exchanger for heterogeneous gas-phase reactions. *Chem. Eng Technol*. 2005;28:337–343.
5. Ponyavin V, Chen YT, Hechanova AE, Wilson M. Numerical modeling of compact high temperature heat exchanger and chemical decomposer for hydrogen production. *Heat Mass Transf*. 2008;44: 1379–1389.
6. Mei FH, Parida PR, Jiang J, Meng WJ, Ekkad SV. Fabrication, assembly, and testing of Cu- and Al-based microchannel heat exchangers. *J Microelectromech Sys*. 2008;17:869–881.
7. Jiang PX, Fan MH, Si GS, Ren ZP. Thermal-hydraulic performance of small scale micro-channel and porous-media heat-exchangers. *Int J Heat Mass Transf*. 2001;44:1039–1051.
8. Kang SW, Tseng SC. Analysis of effectiveness and pressure drop in micro cross-flow heat exchanger. *Appl Thermal Eng*. 2007;27:877–885.
9. Hasan MI, Rageb AA, Yaghoubi M, Homayoni H. Influence of channel geometry on the performance of a counter flow microchannel heat exchanger. *Int J Thermal Sci*. 2009;48:1607–1618.
10. Ranganayakulu C, Seetharamu KN. The combined effects of wall longitudinal heat conduction, inlet fluid flow nonuniformity and temperature nonuniformity in compact tube-fin heat exchangers: a finite element method. *Int J Heat Mass Transf*. 1999;42: 152–162.
11. Chen WL, Yang YC, Lee HL. Three-dimensional pipe fouling layer estimation by using conjugate gradient inverse method. *Num Heat Transf Part A: Appl*. 2009;55:845–865.
12. Alm B, Knitter R, Hausselt J. Development of a ceramic micro heat exchanger design, construction, and testing. *Chem Eng Tech*. 2005; 28:1554–1560.
13. Kwon YC, Kim DH, Lee JH, Choi JY, Lee SJ. Experimental study on heat transfer characteristics of internal heat exchangers for CO_2 system under cooling condition. *J Mech Sci Technol*. 2009;23:698–706.
14. Miwa J, Asako Y, Hong C, Faghri M. Performance of gas-to-gas micro-heat exchangers. *J Heat Transf*. 2009;131:051801-1–051801-9.
15. Chowdhury K, Sarangi S. The effect of variable specific heat of the working fluids on the performance of counterflow heat exchangers. *Cryogenics*. 1984;24:679–680.
16. Peterson RB, Vanderhoff JA. Analysis of a bayonet-type counterflow heat exchanger with axial conduction and radiative heat loss. *Num Heat Transf Part A - Appl*. 2001;40:203–219.
17. Nellis GF. A heat exchanger model that includes axial conduction, parasitic heat loads, and property variations. *Cryogenics*. 2003;43: 523–538.
18. Joshi HM, Webb R. Heat transfer and friction in offset strip-fin heat exchanger. *Int J Heat Mass Transf*. 1987;30:69–84.
19. Ali AHH, Kishinami K, Hanaoka Y, Suzuki J. Numerical study on laminar flow forced-convection heat transfer for air in a channel with offset plates heated by radiation heat flux. *Int J Num Meth Heat Fluid Flow*. 1998;8:539–558.
20. Bier W, Keller W, Linder G, Seidel D, Schubert K, Martin H. Gas to gas heat transfer in micro heat exchangers. *Chem Eng Process*. 1993;32:33–43.
21. Stief T, Langer OU, Schubert K. Numerical investigations of optimal heat conductivity in micro heat exchangers. *Chem. Eng Technol*. 1999;22:297–303.
22. Maranzana G, Perry I, Maillet D. Mini- and micro-channels: influence of axial conduction in the walls. *Int J Heat Mass Transf*. 2004; 47:3993–4004.
23. Meschke F, Riebler G, Hessel V, Schurer J, Baier T. Hermetic gas-tight ceramic microreactors. *Chem Eng Technol*. 2005;28:465–473.
24. Mahulikar SP, Herwig H. Theoretical investigation of scaling effects from macro-to-microscale convection due to variations in incompressible fluid properties. *Appl Phys Lett*. 2005;86: 014105.
25. Luo L, Fan Y, Tondeur D. Heat exchanger: from micro- to multiscale design optimization. *Int J Energy Res*. 2007;31:1266–1274.

26. Mahulikar SP, Herwig H, Hausner O. Study of gas microconvection for synthesis of rarefaction and nonrarefaction effects. *J Microelectromech Sys.* 2007;16:1543–1556.
27. Rachkovskij DA, Kussul EM, Talayev SA. Heat exchange in short microtubes and micro heat exchangers with low hydraulic losses. *Microsys Technol*. 1998;4:151–158.
28. Kadaner YS, Rassadkin YP, Spektor EL. Heat transfer during laminar fluid flow in a pipe with radiative heat removal. *J Eng Phys. (Inzhenerno-Fizicheskii Zhurnal)* 1973;20:31–37.
29. Anderson JD Jr. *Hypersonic and High Temperature Gas Dynamics*. Singapore: McGraw-Hill, 1989:605–609.
30. Howell JR. *A Catalog of Radiation Heat Transfer Configuration Factors*, 2nd ed. New York: McGraw-Hill, 1982; Available at: web-format - http://www.me.utexas.edu/∼howell/.
31. Kakaç S, Liu H. *Heat Exchangers: Selection, Rating and Thermal Design*, 2nd ed. Boca Raton: CRC Press, 2002:45–57.
32. Gad-el-Hak M. The fluid mechanics of microdevices–the Freeman scholar lecture. *J Fluids Eng*. 1999;121:5–33.

Manuscript received Oct. 31, 2009, and revision received Feb. 4, 2010.